Quasiparticle properties of the nonlinear Holstein model at finite doping and temperature

Shaozhi Li, E. A. Nowadnick, and S. Johnston

Phys. Rev. B **92**, 064301 — Published 3 August 2015

DOI: 10.1103/PhysRevB.92.064301

Quasiparticle properties of the non-linear Holstein model at finite doping and temperature

Shaozhi Li,[1] E. A. Nowadnick,[2] and S. Johnston[1]

[1]*Department of Physics and Astronomy, University of Tennessee, Knoxville, Tennessee 37996-1200, USA*
[2]*School of Applied and Engineering Physics, Cornell University, Ithaca, NY 14853 USA*

We use determinant quantum Monte Carlo to study the single particle properties of quasiparticles and phonons in a variant of the two-dimensional Holstein model that includes an additional non-linear electron-phonon (*e-ph*) interaction. We find that a small positive non-linear interaction reduces the effective coupling between the electrons and the lattice, suppresses charge-density wave (CDW) correlations, and hardens the effective phonon frequency. Conversely, a small negative non-linear interaction can enhance the *e-ph* coupling resulting in heavier quasiparticles, an increased tendency towards a CDW phase at all fillings, and a softened phonon frequency. An effective linear model with a renormalized interaction strength and phonon frequency can qualitatively capture this physics; however, the quantitative effects of the non-linearity on both the electronic and phononic degrees of freedom cannot be captured by such a model. These results are significant for typical non-linear coupling strengths found in real materials, indicating that non-linearity can have an important influence on the physics of many *e-ph* coupled systems.

PACS numbers:

I. INTRODUCTION

The electron-phonon (*e-ph*) interaction plays an important role in many systems including conventional metals and superconductors,[1,2] organic semiconductors,[3,4] fullerenes,[5,6] and a large number of transition metal oxides.[7–17] In general, the *e-ph* interaction induces a local distortion of the lattice surrounding a carrier, resulting in quasiparticles dressed by phonon excitations commonly known as polarons. In some cases these lattice distortions can be large and tightly bound to the electron, such that the quasiparticle has a very large effective mass m^* and vanishing quasiparticle residue Z.[18] In this limit, the quasiparticle is typically referred to as a small polaron. In most models, the crossover to the small polaron regime occurs for $\lambda > 1$, where λ parameterizes the (dimensionless) strength of the *e-ph* interaction. When $\lambda < 1$ the carriers are still dressed by the lattice, forming large polarons where the lattice distortions are spread out over many lattice constants[18].

Almost all of our knowledge about the effects of the *e-ph* interaction has been obtained from linear models. The derivation of these models is standard. First, the *e-ph* interaction is expanded in powers of the atomic displacement. This is followed by a truncation of the expansion to linear order under the *assumption* of small lattice displacements. These same models, however, often predict the formation of small polarons or charge-density-wave (CDW) phases for sufficiently large *e-ph* coupling, which are characterized by large lattice displacements. For example, the displacements in the linear Holstein and Hubbard-Holstein models can be on the order of the lattice constant when CDW correlations are significant.[19–21] This can occur even for weak values of the *e-ph* coupling if the Fermi surface is well nested, as is the case for the Holstein model with nearest neighbor hopping on a cubic lattice. Similarly, a small polaron can be dressed by tens to hundreds of phonon quanta,[22] implying the presence of a heavily distorted lattice surrounding the carrier. Clearly, these predictions directly violate the assumptions underlying the linear model, which is an unambiguous sign that important physics has been discarded during its derivation.[23]

These considerations show that the higher order terms in the *e-ph* interaction are likely to be important whenever the linear term is large (or when strong nesting conditions are present). But non-linear and anharmonic effects can also be "switched on" in a weakly coupled system, if the underlying atoms of the lattice are driven far from their equilibrium positions by an external perturbation. For example, several recent experiments have exploited optical pump pulses to drive the lattice, creating large lattice deformations or excited coherent phonon oscillations.[24–27] These excited lattice states can melt various ordered phases[28,29] or may induce transient superconducting states.[30,31] Here, nonlinear and anharmonic phonon dynamics are thought to play a vital role in creating such transient states.[25,30,31]

The first attempts to include higher order terms were made by Adolphs and Berciu (Ref. 23). They considered the effects of non-linear *e-ph* interactions on a single carrier in the Holstein model using the momentum average approximation[22] and found that small non-linear couplings dramatically undress the quasiparticle. This was attributed to a simultaneous hardening of the bare phonon frequency and a renormalization of the bare *e-ph* coupling constant, resulting in an overall weaker effective linear interaction. Later work by some of the present authors considered finite carrier concentrations and temperatures using non-perturbative determinant quantum Monte Carlo (DQMC).[20] Here too, the presence of a non-linear interaction was found to suppress the tendency towards the formation of CDW and superconducting states found in the linear model.

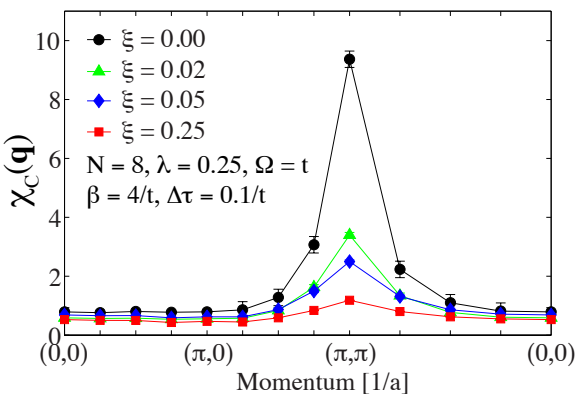

FIG. 1: (color online) The momentum dependence of the charge susceptibility $\chi_C(\mathbf{q})$ as a function of non-linear interaction strength $\xi > 0$. The trends shown here follow those reported in Ref. 20, where the increasing non-linear interaction strength suppresses the CDW correlations in the system. The parameters for the calculation are as indicated. Error bars smaller than the marker size have been suppressed for clarity.

It is important to note that the effects of the non-linear interactions observed in Refs. 20 and 23 are significant, even for relatively small non-linear interaction strengths. This is illustrated in Fig. 1, which shows the suppression of the CDW correlations in the half-filled Holstein model as a function of the non-linear coupling strength. [The degree of non-linearity is indicated by the ratio of the pre-factors of the quadratic (g_2) and linear (g_1) interaction terms $\xi = \frac{g_2}{g_1}$, see Sec. II A.] Here, the charge susceptibility provides a measure of the strength of the CDW correlations. It is defined as

$$\chi_C(\mathbf{q}) = \frac{1}{N^2}\int_0^\beta d\tau \langle \hat{T}_\tau \hat{\rho}(\mathbf{q},\tau)\hat{\rho}^\dagger(\mathbf{q},0)\rangle, \qquad (1)$$

where $\hat{\rho}(\mathbf{q}) = \sum_{i,\sigma} e^{i\mathbf{q}\cdot\mathbf{R}_i}\hat{n}_{i,\sigma}$, and $\hat{T}_\tau$ is the time-ordering operator. In this case, the well-known[32,33] tendency for the linear model to form a $\mathbf{Q} = (\pi/a, \pi/a)$ CDW at half-filling is suppressed for ξ as small as $\sim 0.02 - 0.05$.

The suppression of $\chi_C(\mathbf{q})$ for small ξ is noteworthy because this ratio is typical of many models used to parameterize *e-ph* interactions in real materials. In the transition metal oxides, for example, electrons can couple strongly to oxygen bond stretching modes via the modulation of the near-neighbor transition metal $3d$-oxygen $2p$ (TM-O) hopping integral t_{pd}, which depends on the TM-O bond distance.[13,34] If d is TM-O bond distance and d_0 is its equilibrium value, then this coupling mechanism leads to terms in the Hamiltonian of the form

$$H_{\rm kin} = \sum_{\langle i,j\rangle,\sigma} t_{pd}(d) c^\dagger_{i,\sigma} p_{j,\sigma}, \qquad (2)$$

where the $c_{i,\sigma}$ ($p_{j,\sigma}$) operators act on the TM 3d and O 2p orbitals, respectively. The hopping integral has a typical dependence $t_{pd} \sim (d/d_0)^{-\beta}$, with $\beta = 3.5$.[34] Expanding this dependence to second order in powers of $(d - d_0)$ gives

$$H_{\rm e-ph} = \sum_{\langle i,j\rangle,\sigma} \left[\alpha_1(d-d_0) + \alpha_2(d-d_0)^2\right] c^\dagger_{i,\sigma} p_{j,\sigma}, \quad (3)$$

where $\alpha_1 = -\beta t_{pd}(d_0)/d_0$ and $\alpha_2 = \frac{\beta(\beta+1)t_{pd}(d_0)}{2d_0^2}$. (The zeroth order terms are included in the non-interacting terms of the Hamiltonian). Taking typical values[35] for the various parameters in transition metal oxides, one arrives at a ratio of $|\xi| \sim 0.05$. Therefore real materials have intrinsic non-linear interactions that are large enough to be relevant when the linear coupling is strong. For this particular coupling mechanism the sign of ξ is negative, however, this is not guaranteed for all coupling mechanisms.[36]

In this paper we expand upon our previous work examining the impact of non-linear interactions on the CDW and superconducting phases of the Holstien model.[20] We present results for the single-particle electronic and phononic properties of the model, thus providing a more comprehensive picture of the effects of non-linearity. Since DQMC is formulated in the grand canonical ensemble, we are able to examine these properties at finite temperatures and carrier concentrations for the first time. We find that the inclusion of a non-linear interaction renormalizes both the effective frequency of the Holstein phonon and the effective *e-ph* coupling strength, resulting in significant changes in both the electronic and phononic properties of the model. Furthermore, we demonstrate that while the qualitative effects of the non-linearity can be framed in terms of an effective linear model, the quantitative effects on both the electronic and phononic properties of the model cannot be. This conclusion requires an examination of both the electronic and phononic properties, and thus cannot be arrived at by considering electronic properties only. Our results reenforce the notion that the full non-linearity must be included in order to obtain an accurate picture of both the electronic and phononic degrees of freedom whenever strong linear *e-ph* interactions are present.

II. METHODS

A. The Non-linear Holstein Model

We study a variant of the Holstein model that includes additional non-linear interaction terms. The Hamiltonian is partitioned as

$$H = H_{\rm el} + H_{\rm lat} + H_{\rm int}, \qquad (4)$$

where

$$H_{\rm el} = -t\sum_{\langle i,j\rangle,\sigma} c^\dagger_{i,\sigma} c_{j,\sigma} - \mu\sum_{i,\sigma}\hat{n}_{i,\sigma}, \qquad (5)$$

contains the non-interacting electronic terms,

$$H_{\text{lat}} = \sum_i \left[\frac{\hat{P}_i^2}{2M} + \frac{M\Omega}{2} \hat{X}_i^2 \right] = \sum_i \Omega \left[b_i^\dagger b_i + \frac{1}{2} \right], \quad (6)$$

contains the non-interacting lattice terms, and

$$H_{\text{int}} = \sum_{i,k,\sigma} \alpha_k \hat{n}_{i,\sigma} \hat{X}_i^k = \sum_{i,k,\sigma} g_k \hat{n}_{i,\sigma} (b_i^\dagger + b_i)^k \quad (7)$$

contains the interaction terms to k^{th} order in the atomic displacement. Here, $c_{i,\sigma}^\dagger$ ($c_{i,\sigma}$) creates (annihilates) an electron of spin σ on lattice site i; $b_i^\dagger$ (b_i) creates (annihilates) a phonon on lattice site i; $\hat{n}_{i,\sigma} = c_{i,\sigma}^\dagger c_{i,\sigma}$ is the number operator; μ is the chemical potential; t is the nearest-neighbor hopping integral; M is the ion mass; Ω is the phonon frequency; $\hat{X}_i$ and $\hat{P}_i$ are the lattice position and momentum operators, respectively; and $g_k = \alpha_k (2M\Omega)^{-\frac{k}{2}}$ is the strength of the *e-ph* coupling to k^{th} order in displacement.

The non-linear Holstein model is characterized by several dimensionless parameters, and the specific choice in parameterization is not unique. Here, we follow the convention used in previous works,[20,23] where the usual dimensionless parameter $\lambda = \alpha_1^2/(M\Omega^2 W) = g_1^2/(4t\Omega)$ parameterizes the linear coupling strength and $\xi_k = g_k/g_{k-1}$ parameterizes the non-linear interaction terms. This choice provides a convenient interpretation with large λ implying a strong linear interaction and large ξ_k implying strong non-linear effects. In the linear model ($\xi_k = 0$) $\lambda > 1$ implies the formation of small polarons. Thus this choice of parameterization is also useful for making comparisons to our expectations gained from studying the linear model.

B. Determinant Quantum Monte Carlo

We use DQMC to study the non-linear Holstein model. The details of the method are given in several references (see for example Refs. 37 - 39) and the specifics for handling the lattice degrees of freedom can be found in Refs. 19, 20, and 32.

In our calculations we keep $g_1 > 0$ without loss of generality. Furthermore, Ref. 23 examined terms to 4^{th} order in the interaction and found that the largest effect was produced by the 2^{nd} order terms. We expect a similar result here and restrict ourselves to $k = 2$ while defining $\xi = \frac{g_2}{g_1}$. Furthermore, we neglect the anharmonic terms in the lattice potential, which are not expected to significantly alter our results when $\xi > 0$.[23] (Such terms are needed, however, when ξ is large and negative, see section IIIE.) Throughout this work we examine two-dimensional square lattices with a linear dimension N (a total of $N \times N$ sites) and set $a = t = M = 1$ as our units of distance, energy, and mass, respectively. We typically work on lattice sizes ranging from $N = 4$ to 8 in size. In general we do not observe significant finite size effects,[20] which is likely due to the local nature of the interaction in the model.

The Holstein model and its non-linear extension do not suffer from a fermion sign problem.[38,40] We are therefore able to perform simulations to arbitrarily low temperatures,[20] however, we find that most of the physical properties we are interested in here can be examined for $\beta = 4/t$. We use this temperature for all plots in this work unless stated otherwise and present results for an imaginary time discretization of $\Delta\tau = 0.1/t$. In all of our simulations we have not observed any significant $\Delta\tau$ errors introduced by this choice.

C. Analytic Continuation

The DQMC calculation provides the phonon Green's function $D(\mathbf{q}, \tau) = \langle T \hat{X}_{\mathbf{q}}(\tau) \hat{X}_{-\mathbf{q}}(0) \rangle$ measured on the imaginary time axis. The phonon Green's function is related to the phonon spectral function on the real axis by the integral equation

$$\int_0^\beta d\tau D(\mathbf{q}, \tau) = \int_{-\infty}^{\infty} \frac{d\omega}{2\pi} \frac{B(\mathbf{q}, \omega)}{\omega}. \quad (8)$$

This equation also provides a normalization condition for $B(\mathbf{q}, \omega)$. In section III C we examine the phonon spectral properties of the non-linear Holstein model, which requires that the phonon Green's function be analytically continued to the real frequency axis. This is accomplished with the Maximum Entropy method (MEM).[41] The analytic continuation procedure is identical to the one given in Ref. 42 and the reader can refer to there for details.

MEM requires a model default function to define the entropic prior. We adopt a momentum-independent Lorentzian model, which is peaked at the renormalized phonon frequency predicted by the mean-field treatment of the non-linear interaction $\Omega_{MF} = \Omega + 2g_2$ (see section III D) and of width t. Our results are robust against reasonable changes in this choice of default function.

III. RESULTS AND DISCUSSION

Our results for the single-particle electronic and phononic properties of the non-linear Holstein model are presented in this section. We will begin by first examining the renormalization of the quasiparticles as a function of doping, temperature, and phonon energy. We then examine how the interplay between the quasiparticles and renormalized phonons affect the energetics of the system. Following this, results are presented for the renormalization of the phonons. Finally, after all of these effects are examined, we demonstrate that the simultaneous renormalization of the electronic and phonic subsystems cannot be quantitatively captured by an effective linear model. Combined, these results paint a

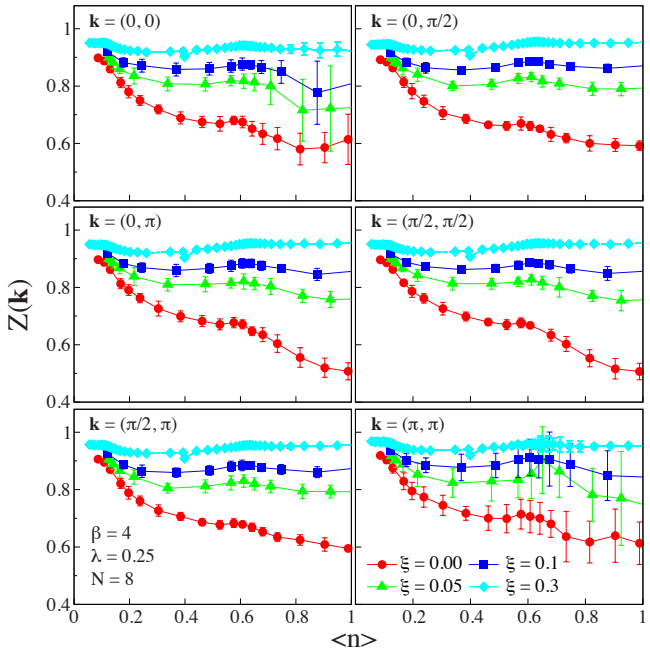

FIG. 2: (color online) The quasiparticle residue $Z(\mathbf{k})$ as a function of band filling $\langle n\rangle$ for (a) $\mathbf{k} = (0,0)$, (b) $(0,\pi/2)$, (c) $(0,\pi)$, (d) $(\pi/2,\pi 2)$, (e) $(\pi/2,\pi)$, and (f) (π,π). Results are shown for various values of the non-linear interaction strength ξ, as indicated in panel (f), and are obtained using an $N = 4\times 4$ cluster with a linear coupling $\lambda = 0.25$ and an inverse temperature $\beta = 4/t$. Error bars smaller than the marker size have been suppressed for clarity.

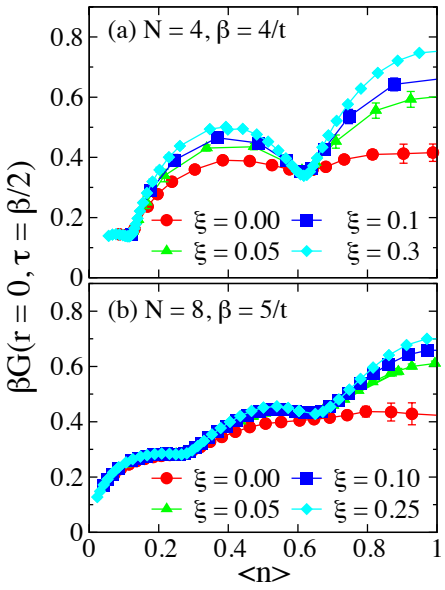

FIG. 3: The spectral weight at the Fermi level given by $\beta G(r=0,\tau=\beta/2) \equiv \beta G_{\beta/2}$ as a function of band filling $\langle n\rangle$ for various values of the non-linear coupling strength ξ. (a) Results for a $N = 4$ cluster and an inverse temperature $\beta = 4/t$. (b) Results for a larger $N = 8$ cluster and a lower temperature $\beta = 5/t$. All results are obtained for a linear coupling $\lambda = 0.25$ and a frequency of $\Omega = t$. Error bars smaller than the markers have been suppressed for clarity.

more detailed picture of how *both* the quasiparticles and phonons are renormalized by the non-linear *e-ph* interaction, which cannot be obtained by examining only one of these subsystems. In the following sections we consider results for the case $\xi > 0$. Considerations of the $\xi < 0$ case are presented in Sec. III E.

A. The quasiparticle residue

We begin by examining the carrier's quasiparticle reside $Z(\mathbf{k})$ as a function of the non-linear coupling strength and doping. This quantity is related to the effective mass via $Z^{-1} \propto \frac{m^*}{m}$. It can be obtained from the imaginary axis self-energy $\Sigma(\mathbf{k}, i\omega_n)$ using the relationship $Z(\mathbf{k}) = \frac{1}{1+b(\mathbf{k})}$,[43] where

$$b(\mathbf{k}) = \lim_{\omega_n\to 0} -\frac{\partial\Sigma'(\mathbf{k}, i\omega_n)}{\partial\omega_n}. \qquad (9)$$

Here, we approximate $b(\mathbf{k})$ by evaluating Eq. (9) for the lowest Matsubara frequency $\omega_n = \pi/\beta$.

Fig. 2 shows $Z(\mathbf{k})$ as a function of carrier concentration for several values of the non-linear coupling ξ. These results were obtained on an $N = 4$ cluster, using a linear coupling strength $\lambda = 0.25$ and $\Omega = t$. In the linear model ($\xi = 0$, red dots) the quasiparticle residue decreases as the filling approaches $\langle n\rangle = 1$, where the $\mathbf{Q} = (\pi,\pi)$ CDW correlations begin to dominate the system (Fig. 1). Note that strong CDW correlations are observed, even for the small value of the linear coupling used here, due to a perfect (π,π) nesting condition in the two-dimensional Fermi surface. (For references, this choice of parameters predicts a CDW transition temperature $\beta_c \sim 5.2/t$ on an $N = 8$ cluster for the linear model, obtained from extrapolating $1/\chi_C(\mathbf{q})$ to zero as a function of β.) This nesting condition also results in large lattice displacements in the linear model. As a result, the inclusion of the non-linear terms has a significant effect on the quasiparticle residue where, for $\xi > 0$, a significant undressing of the quasiparticles occurs and the quasiparticle residues at all momenta begin to rise. This occurs at all doping, however, the effect is more pronounced near half-filling. (Our $\xi = 0$ results are in good agreement with Ref. 44, which examined larger system sizes using a complementary diagrammatic Monte Carlo method.)

The formation and suppression of the CDW gap is also reflected in the spectral weight at the Fermi level, which can be obtained from the local imaginary time Green's function $\beta G(r=0,\tau=\beta/2) \equiv \beta G_{\beta/2}$.[45] Fig. 3a plots $G_{\beta/2}$ as a function of filling $\langle n\rangle$ for the same parameters used in Fig. 2. Fig. 3b plots similar results obtained on a larger cluster and at lower temperature, where the qualitative behavior is the same. The spectral weight in the linear model initially grows with increasing car-

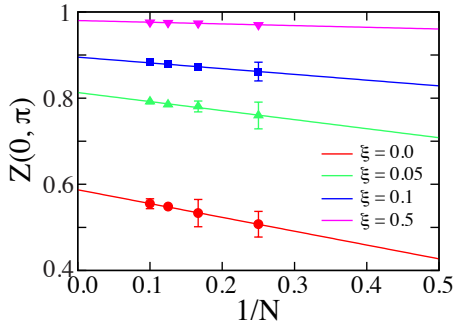

FIG. 4: (color online) A finite size scaling analysis of $Z(0,\pi)$ as a function of $1/N$ where N is the linear dimension of the cluster. The parameters for the calculations are $\beta = 4/t$, $\Omega = t$, and $\lambda = 0.25$. Error bars smaller than the marker size have been suppressed for clarity.

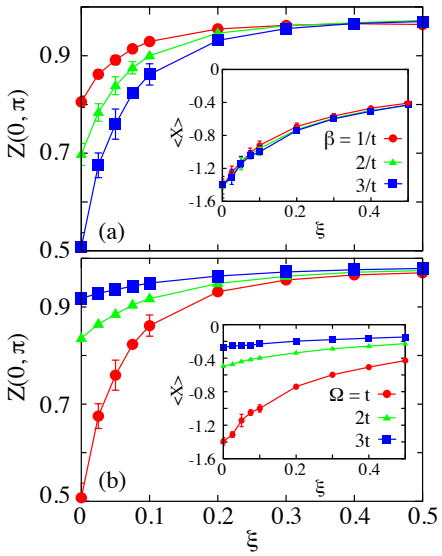

FIG. 5: The (a) temperature and (b) Ω dependence of the quasiparticle residue in the half-filled model as a function of non-linear coupling strength ξ. The insets show the corresponding expectation value of the lattice displacement. All results are obtained on an $N = 4$ cluster and with a linear coupling $\lambda = 0.25$. Error bars smaller than the marker size have been suppressed for clarity.

rier concentration, but saturates as the concentration approaches half-filling and CDW correlations begin to dominate. When a non-linear interaction is introduced, however, $G_{\beta/2}$ increases at most fillings, which is most pronounced near $\langle n\rangle \sim 1$. (The dip around $\langle n\rangle = 0.6$ is a finite size effect due to the smaller number of momentum points in the $N = 4$ cluster. It is much less pronounced on the larger $N = 8$ cluster.) This spectral weight increase directly reflects the increase in the quasiparticle residue and the suppression of the CDW correlations. Previously we showed that a large non-linear coupling drives the system into a metallic state at half-filling, with the value of $\beta G_{\beta/2}$ approaching the non-interacting value.[20] The results in Fig. 3 indicate that this also occurs for carrier concentrations away from half-filling.

The results presented in Figs. 2 and 3a are obtained on a $N = 4$ cluster; however, they are qualitatively representative of the results obtained for all examined cluster sizes, as hinted at by comparing Figs. 3a and 3b. To confirm this, in Fig. 4 we perform a finite size scaling analysis for $Z(0,\pi)$ at half-filling, where the reduction in Z by CDW correlations is most pronounced. From this analysis it is clear that the qualitative behavior is not affected by finite size effects and survives in the thermodynamic limit. Moreover, the more pronounced finite size effects occur when the non-linear interaction is weak. As similar scaling results were obtained for both the charge susceptibility and the electron spectral weight in our previous work,[20] we conclude that the qualitative physics of the non-linear model can be obtained on an $N = 4$ cluster.

In Fig. 5a we consider the temperature dependence of $Z(\mathbf{k})$ and average displacement of the lattice $\langle X\rangle = \frac{1}{N^2 L}\sum_{i=1}^{N}\sum_{l=1}^{L} X_{i,l}$ for the half-filled model. Here, results for $Z(0,\pi)$ only are shown, since similar trends were found at all momenta. Focusing first on the linear model, we find that $Z(0,\pi)$ decreases with temperature as the CDW correlations begin to set in. The average lattice displacement, however, does not exhibit the same temperature dependence (see inset of Fig. 5a).[46] As the non-linear interaction strength grows, however, the quasiparticle residue increases back towards its non-interacting value. For small ξ this rise is somewhat rapid, but it gives way to a more gradual increase for $\xi \gtrsim 0.1$. The increase is also accompanied by a decrease in the average lattice displacement (inset of Fig. 5). This behavior mirrors the observed ξ-dependence of the CDW susceptibility,[20] and is consistent with the conclusion that a finite $\xi > 0$ undresses the carriers and relaxes the lattice distortions normally present in the linear model.

The Ω-dependence of $Z(\pi,0)$ and $\langle X\rangle$ for the same model are shown in Fig. 5b. Here, the $\xi = 0$ results are consistent with those obtained for the 1D Holstein model, where the tendency to form a CDW grows with decreasing phonon frequencies.[47] Consequently, both the quasiparticle residue and average lattice displacement decrease as the value of Ω increases. The introduction of $\xi > 0$ results in the further decrease in these quantities.

From this section we conclude that the non-linear interaction with $\xi > 0$ acts to undress the quasiparticles and that this is a generic result, regardless of the values of Ω and β. The undressing, however, is much more pronounced at low temperatures, for smaller values of the phonon frequency, and near half-filling, where the CDW correlations (and subsequently the local lattice displacements) are largest in the linear model.

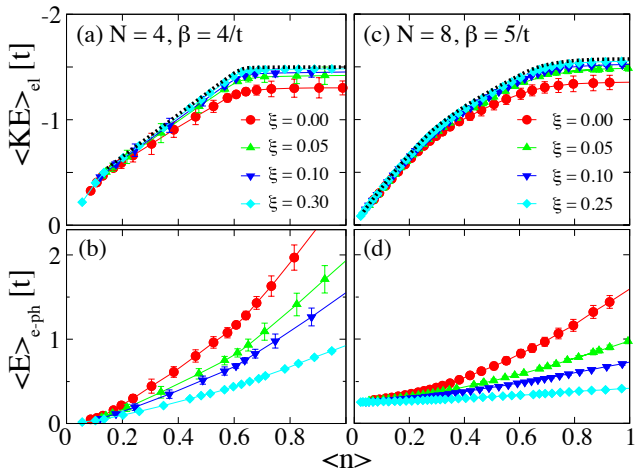

FIG. 6: (color online) (a) The electron kinetic energy $\langle \mathrm{KE}\rangle_{\mathrm{el}}$ and (b) the *e-ph* energy $\langle \mathrm{E}\rangle_{\mathrm{e-ph}}$ as a function of band filling $\langle n\rangle$ for various non-linear interaction strengths ξ, as indicated. Results are obtained on an $N = 4$ cluster and with a linear coupling $\lambda = 0.25$, phonon frequency $\Omega = t$, and an inverse temperature $\beta = 4/t$. The dashed lines in panels (a) and (c) indicate the non-interacting result. (c) and (d) show corresponding results for a larger $N = 8$ cluster and $\beta = 5/t$. The remaining parameters are the same as in (a) and (b). Error bars smaller than the marker size have been suppressed for clarity.

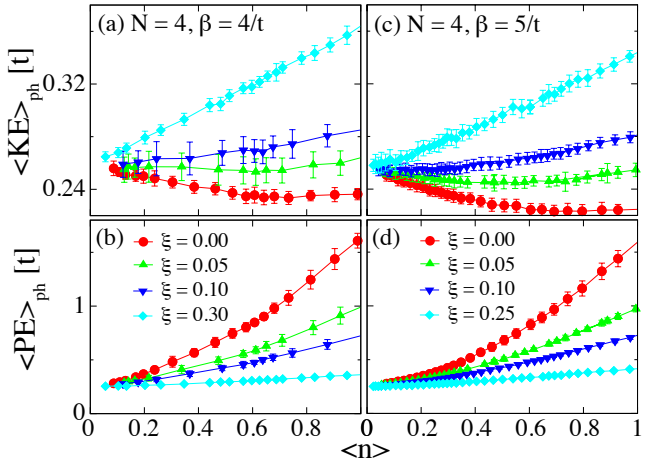

FIG. 7: (color online) The phonon (a) kinetic energy $\langle \mathrm{KE}\rangle_{ph}$ and (b) potential energy $\langle PE\rangle_{ph}$ as a function of band filling $\langle n\rangle$ for various of the non-linear interaction strength ξ, as indicated in panel (b). Results are obtained on an $N = 4$ cluster and with a linear coupling $\lambda = 0.25$, $\Omega = 1$,and $\beta = 4/t$. (c) and (d) show similar results obtained on a larger $N = 8$ cluster with $\beta = 5/t$. Error bars smaller than the marker size have been suppressed for clarity.

B. Electron and Phonon energetics

The average kinetic energy of the electronic subsystem $\langle \mathrm{KE}\rangle_{\mathrm{el}} = -t\sum_{\langle i,j\rangle,\sigma}\langle c^{\dagger}_{i,\sigma}c_{j,\sigma}\rangle$ at $\beta = 4/t$ is shown in Fig. 6. Results are shown as a function of band filling $\langle n\rangle$ for various ξ and for a linear coupling $\lambda = 0.25$. For $\xi = 0$ the total kinetic energy $-\langle \mathrm{KE}\rangle_e$ increases as a function of $\langle n\rangle$ as higher momentum states are populated in the Fermi sea, however, the total kinetic energy saturates as the filling increases beyond $\langle n\rangle > 0.6$. This is due to the saddle point in the band dispersion at $(0, \pi)$ and is also present in the non-interacting model (indicated by the dashed line). When the non-linear interaction is added we see an overall increase in the total kinetic energy, which tends towards the non-interacting value at all fillings for large ξ. This again reflects the undressing of the quasiparticles and the subsequent increase in mobility of the electronic subsystem.

Fig. 6b shows the corresponding *e-ph* interaction energy, defined as $\langle \mathrm{E}\rangle_{\mathrm{e-ph}} = \sum_i\langle g_1\hat{n}_i\hat{X}_i + g_2\hat{n}_i\hat{X}_i^2\rangle$. Unsurprisingly, the total *e-ph* interaction energy increases with band filling as both the average number of electrons per site and the average lattice displacement increase. This is most evident in the linear model ($\xi = 0$). Increasing the value of ξ naturally leads to smaller lattice displacements and a significant decrease in $\langle \mathrm{E}\rangle_{\mathrm{e-ph}}$.

The average kinetic $\langle \mathrm{KE}\rangle_{\mathrm{ph}}$ and potential $\langle \mathrm{PE}\rangle_{\mathrm{ph}}$ energies of the lattice are shown in Figs. 7a and 7b, respectively. They are given by

$$\langle \mathrm{KE}\rangle_{\mathrm{ph}} = \frac{1}{2\Delta\tau} - \frac{M}{2}\Big\langle \sum_{i,l}\left(\frac{X_{i,l+1} - X_{i,l}}{\Delta\tau}\right)^2\Big\rangle \quad (10)$$

$$\langle \mathrm{PE}\rangle_{\mathrm{ph}} = \frac{M\Omega^2}{2}\Big\langle \sum_{i,l} X_{i,l}^2\Big\rangle. \quad (11)$$

(The factor of $\frac{1}{2\Delta\tau}$ appearing in Eq. (10) is a Euclidean correction introduced by the Wick rotation to the imaginary-time axis.[19])

In the linear model we see a very weak variation in the phonon kinetic energy as a function of filling, with a slight decrease observed near half-filling when the CDW correlations increase. This is consistent with prior observations of the lattice kinetic energy in the vicinity of a CDW transition in the Hubbard- Holstein model.[19] The average potential energy of the lattice grows as the average number of carriers per site increases. When the non-linearity is introduced and the lattice distortions diminish (see 5b, inset), we see an increase in the lattice kinetic energy, which is attributed to the hardening of the phonon dispersion. At the same time, we see a decrease in the total lattice potential energy. Here, the non-linear interaction has two opposing effects: the increase in the phonon frequency increases the lattice potential energy while the decrease in the effective linear coupling decrease the net lattice distortions and subsequently lowers the potential energy. Our results indicate that the latter effect has the stronger impact.

The energetics reported here are completely consistent with the conclusion that the non-linear interaction acts to harden the phonon frequency and weaken the effective

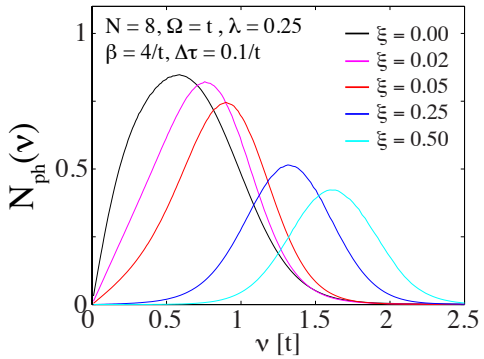

FIG. 8: (color online) The phonon density of states $N_{\rm ph}(\nu) = \frac{1}{N}\sum_{\mathbf{q}} B(\mathbf{q},\nu)$ for the half-filled model as a function of the non-linear interaction strength. The remaining calculation parameters are as indicated.

linear interaction, which results in an undressing of the quasiparticles for $\xi > 0$.

C. Phonon Spectral Properties

In the linear Holstein model the formation of the CDW phase is accompanied by a softening of the phonon dispersion to zero energy at the nesting wavevector $\mathbf{Q} = 2\mathbf{k}_F = (\pi,\pi)$.[42,48–50] This softening is generated by the strong nesting condition of the non-interacting Fermi surface. The inclusion of the non-linear *e-ph* interaction is therefore expected to modify the phonon dispersion in two important ways: first, it will undo the softening at $\mathbf{Q}$ as the CDW correlations are suppressed. Second, it will result in an overall renormalization of the phonon frequency, as discussed in the introduction. We confirm these expectations in this section by examining the phonon spectral function $B(\mathbf{q},\nu)$ and the phonon density of states (DOS) $N_{ph}(\nu) = \frac{1}{N^2}\sum_{\mathbf{q}} B(\mathbf{q},\nu)$.

In the non-interacting limit, $B(\mathbf{q},\nu)$ and $N_{ph}(\nu)$ are delta functions centered at the bare phonon frequency Ω. In the presence of a non-zero linear interaction only, this distribution shifts to lower energy and broadens. This is illustrated in Figs. 8 and 9a, which plot $N_{ph}(\nu)$ and the momentum-resolved phonon spectral function $B(\mathbf{q},\nu)$, respectively, for the half-filled model. These results were obtained on $N = 8$ clusters, with a linear coupling $\lambda = 0.25$, $\Omega = t$, and at an inverse temperature of $\beta = 4/t$. Due to the finite value of λ, the phonon frequency softens from its non-interacting value and $N_{ph}(\nu)$ for the linear model consists of a broad, asymmetric distribution centered at $\sim 0.60t$. The asymmetry in $N_{ph}(\nu)$ reflects the momentum dependence of the softening and the low-energy spectral weight in $B(\mathbf{Q},\nu)$, coupled with the requirement that $B(0) = 0$ for bosons. This is more easily seen in the momentum-resolved spectral function (Fig. 9a), which has a clear Kohn anomaly at $\mathbf{Q} = (\pi,\pi)$.

Two prominent changes occur when $\xi \neq 0$. First, the peak in the DOS shifts to higher energies, which verifies the hardening of the effective phonon frequency. This behavior is also clearly seen in the momentum resolved spectral functions, shown in Fig. 9. Second, the pronounced Kohn anomaly begins to disappear as the CDW correlations are suppressed with increasing values of ξ. Both of these results confirm our expectations.

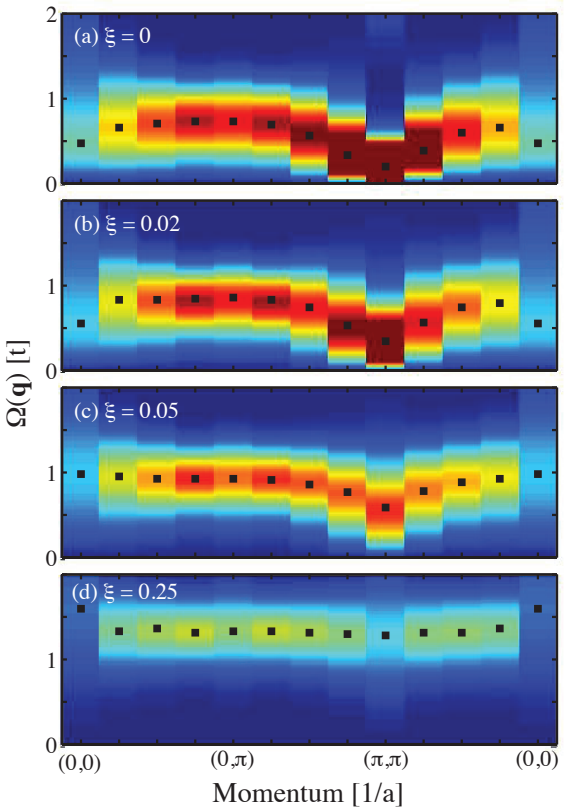

FIG. 9: (color online) The momentum resolved phonon spectral function $B(\mathbf{q},\nu)$ for the half-filled model and for various values of the non-linear interaction strength, as indicated in each panel. Results were obtained on an $N = 8$ cluster with $\lambda = 0.25$, $\Omega = t$, $\beta = 4/t$ and $\Delta\tau = 0.1/t$. The black squares indicate the position of the peak in the phonon spectral function.

D. Mean-field Treatment of the quadratic *e-ph* interaction

As we have repeatedly seen, the non-linear *e-ph* interaction acts to renormalize both the bare linear interaction strength λ and the bare phonon frequency Ω. Both of these effects can be *qualitatively* understood at the mean-field (MF) level for the quadratic model, where an effective linear Hamiltonian is obtained by performing a MF decoupling of the interaction terms proportional to $b_i^\dagger b_i^\dagger$ and $b_i b_i$.[23] The resulting effective MF Hamiltonian

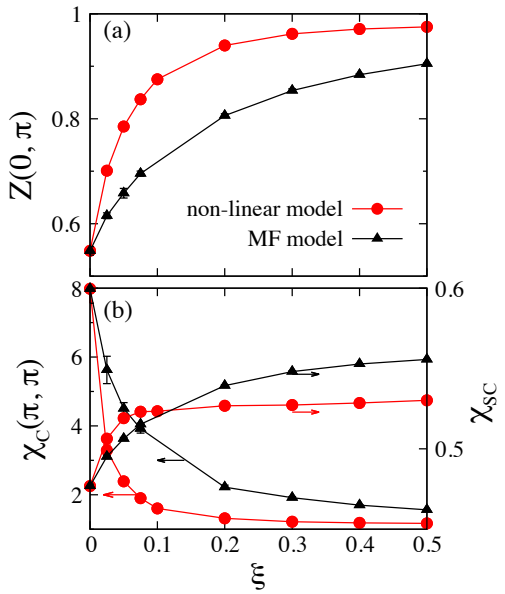

FIG. 10: (color online) A comparison of (a) the quasiparticle residue and (b) CDW $\chi_C(\pi,\pi)$ and pair field susceptibilities χ_{SC} obtained from the non-linear model and its effective linear model, as defined in the main text. The bare linear coupling and phonon frequency are $\lambda = 0.25$ and $\Omega = t$, respectively. In both cases results are obtained on an $N = 8$ cluster and at an inverse temperature of $\beta = 4/t$. Error bars smaller than the marker size have been suppressed for clarity.

is

$$H_{MF} = H_{el} + \sum_i \Omega_{MF}\left(b_i^\dagger b_i + \frac{1}{2}\right) + \sum_{i,\sigma} g_{MF}\hat{n}_{i,\sigma}\left(b_i^\dagger + b_i\right), \quad (12)$$

where $\Omega_{MF} = \Omega + 2g_2$ and $g_{MF} = g_1(1 - \frac{2g_2}{\Omega+4g_2})$ are the renormalized phonon frequency and *e-ph* coupling constants, respectively. One immediately sees that the quadratic *e-ph* interaction leads to a softening (hardening) of the phonon frequency and an increase (decrease) in the effective linear interaction strength g_1 for $\xi < 0$ ($\xi > 0$). These two effects combine to produce an overall increase (decrease) in the strength of the effective dimensionless coupling $\lambda_{eff} \propto \frac{g_{MF}^2}{\Omega_{MF}}$.

The MF treatment of the non-linear interaction is consistent with the general trends reported here and in Refs. 20 and 23. We stress, however, that the MF description only provides a qualitative picture of the non-linear effects. To illustrate this, we compare our DQMC results for the full non-linear Hamiltonian against the predictions obtained from two sets of effective linear models. The first is the MF-derived model defined by Eq. (12). The second is the set of effective linear models whose parameters are obtained by tuning the Ω_{eff} and g_{eff} to reproduce the electronic properties of the system.

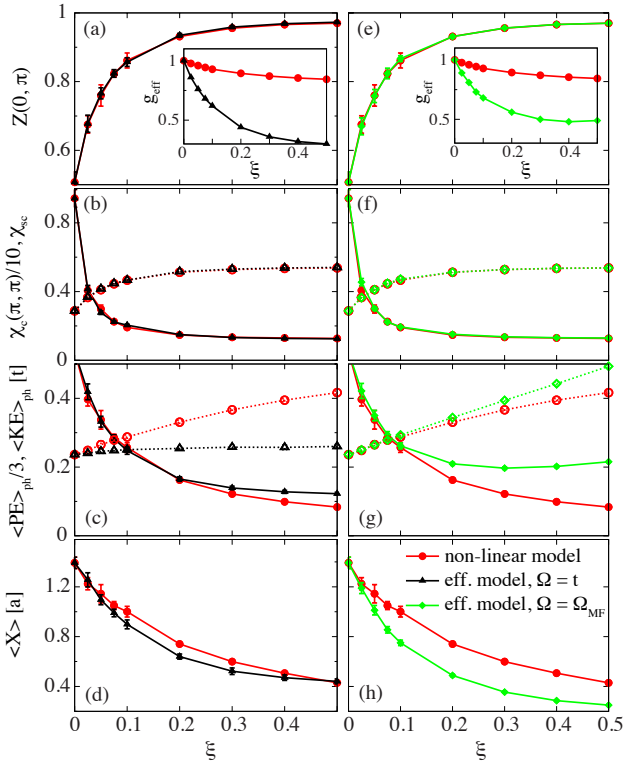

FIG. 11: (color online) A comparison of the results obtained for the full non-linear model and an effective linear model where the value of the *e-ph* coupling constant has been adjusted to reproduce the electronic properties of the non-linear model. Panels (a)-(d) show a comparison for an effective linear model with $\Omega = t$, equal to the bare phonon frequency. Panels (e)-(f) show a comparison for an effective linear model with $\Omega = \Omega_{MF}$. The top row [panels (a) & (e)] compares the quasiparticle residues obtained with both models. The second row [panels (b) & (f)] shows the resulting charge (solid lines) and pair-field (dashed lines) susceptibilities. The third row [panels (c) & (g)] show the resulting phonon potential and kinetic energies. The potential energy has been divided by a factor of three and is indicated by the solid lines while the kinetic energy is indicated by the dashed lines. Finally, the bottom row [panels (d) & (h)] show the average value of the lattice displacement. The remaining parameters of the simulation are $\beta = 4/t$ and $N = 8$.

We consider the MF-derived model first. Fig. 10 compares the results for the quasiparticle residue, $\chi_C(\pi,\pi)$, and the pair-field susceptibility χ_{SC} calculated using the full non-linear model [Eq. (4)] to results obtained from a DQMC simulation of the corresponding MF-derived linear model [Eq. (12)] at half-filling. We find that the MF model does a poor job in quantitatively capturing the electronic properties; it underestimates both the quasiparticle residue $Z(0,\pi)$ and the tendency towards the formation of a CDW when compared to the full non-linear model. The MF model also over-predicts the magnitude of the superconducting pair-field susceptibility when ξ is large and under-predicts it when ξ is small.

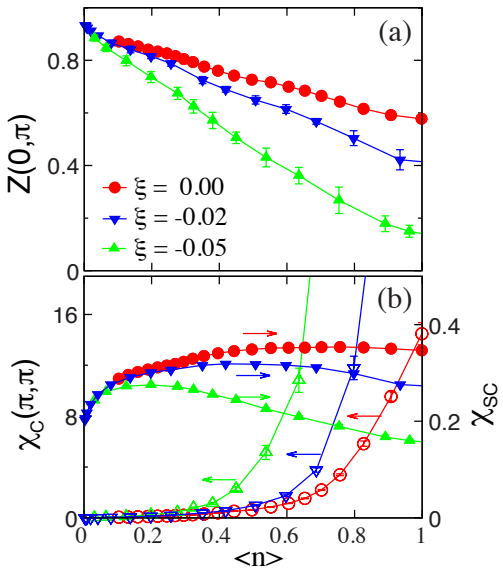

FIG. 12: (color online) (a) the quasiparticle residue and (b) CDW $\chi_C(\pi,\pi)$ (open symbols) and pair field susceptibilities χ_{SC} (solid symbols) as a function of band filling. The parameters are set as: $\lambda = 0.25$, $\Omega = 2t$, $\beta = 4$. The results are obtained on an $N = 8$ cluster. Error bars smaller than the marker size have been suppressed for clarity.

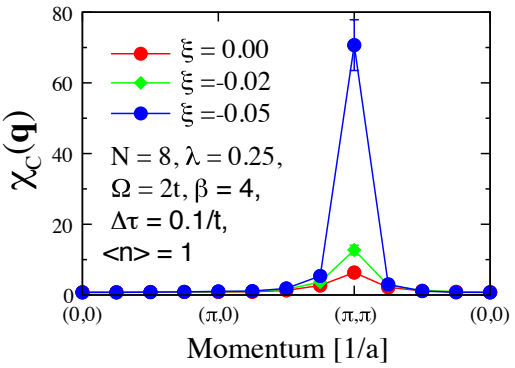

FIG. 13: (color online) The momentum dependence of the charge susceptibility $\chi(\mathbf{q})$ as a function of non-linear interaction strength $\xi < 0$ at half filling. The parameters are set as: $\lambda = 0.25$, $\Omega = 2t$, $\beta = 4$. The results are obtained on an $N = 8$ cluster. Error bars smaller than the marker size have been suppressed for clarity.

The results shown in Fig. 10 demonstrate that the MF treatment of the quadratic interaction can only provide a qualitative picture of the physics of the non-linear model; however, another choice in effective model might do a better job. We explored this possibility by adjusting the effective coupling strength in the linear model such that the linear model reproduce the electronic properties of the full non-linear model. This procedure was performed for two choices in the phonon frequency. First, we set the phonon frequency equal to the bare value and adjusted the value of the coupling strength to reproduce the quasiparticle residue, as shown Fig. 11a. The value of the linear coupling strength g_{eff} needed to produce this agreement is shown in the inset (black solid $\triangle$), where it is compared against the corresponding value of $g_{MF} = g_1 + 2g_2$. By tuning the value of g_{eff} we are able to accurately capture the quasiparticle residue. The charge and superconducting pair-field susceptibilities are also well reproduced, indicating that this effective model is capable of capturing the electronic properties of the system. But when we examine the phonon properties (Figs. 11c & 11d) we find some disagreement, particularity with respect to the predicted kinetic energy of the lattice, where the linear model systematically underpredicts the correct results.

The comparison between the two models can be improved somewhat if we set the phonon frequency to be equal to Ω_{MF} and again readjust the value of g_{eff}. This case is shown in Fig. 11e-h. Using this choice we are again able to accurately capture the electronic properties and improve the comparison between the kinetic energy. But this comes at the expense of the level of agreement between the average lattice potential energy and the average lattice displacement. From this we conclude that an effective linear model cannot capture both the electronic and phononic properties of the non-linear model, for a fixed value of the phonon frequency. These results show that while the *qualitative effects* can be understood using an effective linear model, the full non-linear interaction should be retained if one wishes to accurately capture the effects of the non-linear interaction on both the phononic and electronic properties of the system. A similar conclusion was reached in Ref. 23 in the single carrier limit.

E. Negative values of ξ

We have shown that a positive ($\xi > 0$) non-linear coupling results in a hardening of the phonon frequency and a renormalization of the effective linear *e-ph* coupling to weaker values. But what about the case when $\xi < 0$, where the MF model predicts an enhanced effective linear coupling? Before examining this case, we note that a large negative ξ necessarily requires the inclusion of additional anharmonic terms in the lattice potential.[36] For $\xi < 0$ ($g_2 < 0$) the phonon frequency given by $\Omega_{eff} = \Omega + 2g_2$ can become negative for sufficiently large values of g_2, indicating an instability in the lattice. In this event the anharmonic terms of the lattice potential are required to maintain stability. At present, our codes do not contain such terms and we are unable to examine this case in great detail. We therefore restrict ourselves to a larger value of $\Omega = 2t$ and small values of $|g_2|$ in order to get a feel for the $g_2 < 0$ regime while ensuring the stability of the lattice.

Fig. 12a shows the quasiparticle residue, $\chi_C(\pi,\pi)$, and

χ_{SC} as a function of band filling for various values of $\xi < 0$. These results were obtained for a linear coupling of $\lambda = 0.25$ and on an $N = 8$ cluster. We find that the quasiparticles are more effectively dressed when $\xi < 0$, and the quasiparticle residue is much smaller for all fillings when increasing negative quadratic interactions are included. The CDW correlations are also significantly enhanced, as reflected in the charge susceptibility shown in Fig. 12b. Both of these observations are in line with the expected increase in the effective linear coupling. Furthermore, since the CDW phase directly competes with s-wave superconductivity, the pair-field susceptibility is suppressed at filling values where the CDW correlations dominate. In addition, we also see a noticeable decrease in the pair-field susceptibility at band fillings where the CDW does not dominate. This suggests that the negative non-linear interaction has a detrimental effect on the superconducting transition temperature, which stems from the decrease in the quasiparticle residue. Fig. 13 plots the momentum dependence of the charge susceptibility $\chi(\mathbf{q})$ as a function of negative ξ at half filling, where it is clear that the dominant CDW correlations are still being set by the Fermi surface nesting condition.

IV. SUMMARY AND CONCLUSIONS

We have examined the role of non-linear *e-ph* interactions in shaping the single-particle electronic and phononic properties of quasiparticles in the Holstein model at finite carrier concentrations and temperatures using DQMC. We find that the inclusion of a positive non-linear interaction term serves to undress the quasiparticles leading to carriers with lighter effective masses. This leads to changes in the energetics of both the electrons and phonons, as well as the relaxation of the local lattice distortions surrounding each carrier. This is due to a simultaneous hardening of the phonon frequency and renormalization of the effective linear coupling to smaller values. We have also examined the case when the quadratic *e-ph* interaction has the opposite sign as the linear interaction, although this case cannot be explored in detail without the inclusion of additional anharmonic terms in the lattice potential. Nevertheless, in our limited range of accessible parameters, we find that a quadratic interaction results in an increased dressing of the carriers and an enhanced tendency towards the formation of a $\mathbf{Q} = (\pi, \pi)$ CDW ordered phase.

While many of the effects we have discussed can be understood qualitatively at the mean-field level, we have demonstrated that the quantitative effects can only be captured by the full non-linear model. Specifically, the effective linear models fail to simultaneously capture the electronic and phononic properties. Therefore the full non-linear model must be retained if one wishes to accurately capture the properties of the electrons and the phonons. Our results are in good agreement with the results obtained in the single particle limit,[23] and show that non-linearities are relevant at finite carrier concentrations.

Acknowledgments

We thank C. P. J. Adolphs and M. Berciu for useful discussions. This work is partially supported by the Science Alliance Joint Directed Research and Development (JDRD) program. CPU time for this work was provided in part by resources supported by the University of Tennessee and Oak Ridge National Laboratory Joint Institute for Computational Sciences (http://www.jics.utk.edu).

[1] G. Grüner, *The dynamics of charge-density waves*. Rev. Mod. Phys., **60** 1129 (1988).

[2] For example, see Vol. 1 and 2 of *Superconductivity*, edited by R. D. Parks. Dekker, New York, (1969).

[3] Nenad Vukmirović, C. Bruder, and Vladimir M. Stojanović, *Electron-Phonon Coupling in Crystalline Organic Semiconductors: Microscopic Evidence for Nonpolaronic Charge Carriers*. Phys. Rev. Lett. **109**, 126407 (2012);

[4] Shaozhi Li, Xianfeng Dong, Ding Yi, Shijie Xie, *Theoretical investigation on magnetic field effect in organic devices with asymmetrical molecules*. Organic Electronics **14**, 9 (2013).

[5] O. Gunnarsson, *Superconductivity in fullerides*. Rev. Mod. Phys. **69**, 575 (1997).

[6] P. Durand, G. R. Darling, Y. Dubitsky, A. Zaopo, and M. J. Rosseinsky, *The Mott-Hubbard insulating state and orbital degeneracy in the superconducting C_{60}^3- fulleride family* Nat. Mater. **2**, 605 (2003).

[7] A. Lanzara, P. V. Bogdanov, X. J. Zhou, S. A. Kellar, D. L. Feng, E. D. Lu, T. Yoshida, H. Eisaki, A. Fujimori, K. Kishio, J. I. Shimoyama, T. Noda, S.Uchida, Z. Hussain, and Z. X. Shen, *Evidence for ubiquitous strong electron-phonon coupling in high-temperature superconductors*. Nature **412**, 510 (2001).

[8] T. Cuk, F. Baumberger, D. H. Lu, N. Ingle, X. J. Zhou, H. Eisaki, N. Kaneko, Z. Hussain, T. P. Devereaux, N. Nagaosa, and Z.-X. Shen, *Coupling of the B_{1g} Phonon to the Antinodal Electronic States of $Bi_2Sr_2Ca_{0.92}Y_{0.08}Cu_2O_{8+\delta}$*. Phys. Rev. Lett. **93**, 117003 (2004); T. P. Devereaux, T. Cuk, Z.-X. Shen, and N. Nagaosa, *Anisotropic Electron-Phonon Interaction in the Cuprates*. Phys. Rev. Lett. **93**, 117004 (2004).

[9] P. D. C. King, T. Takayama, A. Tamai, E. Rozbicki, S. Mckeown Walker, M. Shi, L. Patthey, R. G. Moore, D. Lu, K. M. Shen, H.Takagi, and F. Baumberger, *Spectroscopic indications of polaronic behavior of the strong spin-orbit insulator $Sr_3Ir_2O_7$* Phys. Rev. B **87**, 241106 (2013).

[10] H. J. Park, C. H. Sohn, D. W. Jeong, G. Cao, K. W. Kim, S. J. Moon, Hosub Jin, Deok-Yong Cho, and T. W. Noh, *Phonon-assisted optical excitation in the narrow bandgap*

Mott insulator $Sr_3Ir_2O_7$ Phys. Rev. B **89**, 155115 (2014).

[11] M. Medarde, P. Lacorre, K. Conder, F. Fauth, and A. Furrer, *Giant ^{16}O-^{18}O Isotope Effect on the Metal-Insulator Transition of $RNiO_3$ Perovskites (R =Rare Earth).* Phys. Rev. Lett. 80, 2397 (1998).

[12] H. Park, A. J. Millis, and C. A. Marianetti, *Site-Selective Mott Transition in Rare-Earth-Element Nickelates.* Phys. Rev. Lett. **109**, 156402 (2012).

[13] S. Johnston, A. Mukherjee, I. Elfimov, M. Berciu, and G. A. Sawatzky, *Charge Disproportionation without Charge Transfer in the Rare-Earth-Element Nickelates as a Possible Mechanism for the Metal-Insulator Transition.* Phys. Rev. Lett. **112**, 106404 (2014).

[14] R. Jaramillo, Sieu D. Ha, D. M. Silevitch, Shriram Ramanathan, *Origins of bad-metal conductivity and the insulatormetal transition in the rare-earth nickelates.* Nature Physics, **10**, 304 (2014).

[15] N. Mannella, W. L. Yang, X. J. Zhou, H. Zheng, J. F. Mitchell, J. Zaanen, T. P. Devereaux, N. Nagaosa, Z. Hussain, and Z.-X. Shen, *Nodal quasiparticle in pseudogapped colossal magnetoresistive manganites.* Nature **438**, 474 (2005).

[16] W. S. Lee, S. Johnston, B. Moritz, J. Lee, M. Yi, K. J Zhou, T. Schmitt, L. Patthey, V. Strocov, K. Kudo, Y. Koike, J. van den Brink, T. P. Devereaux, and Z. X. Shen, *Role of Lattice Coupling in Establishing Electronic and Magnetic Properties in Quasi-One-Dimensional Cuprates.* Phys. Rev. Lett. **110**, 265502 (2013).

[17] L. L. Lev, J. Krempaský, U. Staub, V. A. Rogalev, T. Schmitt, M. Shi, P. Blaha, A. S. Mishchenko, A. A. Veligzhanin, Y. V. Zubavichus, M. B. Tsetlin, H. Volfová, J. Braun, J. Minár, and V. N. Strocov, *Fermi Surface of Three-Dimensional $La_{1x}Sr_xMnO_3$ Explored by Soft-X-Ray ARPES: Rhombohedral Lattice Distortion and its Effect on Magnetoresistance* Phys. Rev. Lett. **114**, 237601 (2015)

[18] For a review, see J. T. Devreese, *Polarons.* Encycl. Appl. Phys., **14** 383 (1996).

[19] S. Johnston, E. A. Nowadnick, Y. F. Kung, B. Moritz, R. T. Scalettar, and T. P. Devereaux, *Determinant quantum Monte Carlo study of the two-dimensional single-band Hubbard-Holstein model.* Phys. Rev. B **87**, 235133 (2013).

[20] S. Li and S. Johnston, *The effects of non-linear electron-phonon interactions on superconductivity and charge-density-wave correlations.* Europhys. Lett. **109**, 27007 (2015).

[21] H. A. Craig, C. N. Varney, W. E. Pickett, and R. T. Scalettar, *Static versus dynamic fluctuations in the one-dimensional extended Hubbard model.* Phys. Rev. B **76**, 125103 (2007).

[22] M. Berciu, *Green's Function of a Dressed Particle.* Phys. Rev. Lett. **97**, 036402 (2006); M. Berciu and G. L. Goodvin, *Systematic improvement of the momentum average approximation for the Green's function of a Holstein polaron.* Phys. Rev. B **76**, 165109 (2007).

[23] C. P. J. Adolphs and M. Berciu, *Going beyond the linear approximation in describing electron-phonon coupling: Relevance for the Holstein model.* Europhys. Lett. **102**, 47003 (2013).

[24] M. Först, C. Manzoni, S. Kaiser, Y. Tomioka, Y. Tokura, R. Merlin, and A. Cavalleri, *Nonlinear phononics as an ultrafast route to lattice control.* Nature Physics **7**, 854 (2011).

[25] A. Subedi, A. Cavalleri, and A. Georges, *Theory of nonlinear phononics for coherent light control of solids.* Phys. Rev. B **89**, 220301(R) (2014).

[26] E. Papalazarou, J. Faure, J. Mauchain, M. Marsi, A. Taleb-Ibrahimi, I. Reshetnyak, A. van Roekeghem, I. Timrov, N. Vast, B. Arnaud, and L. Perfetti, *Coherent Phonon Coupling to Individual Bloch States in Photoexcited Bismuth.* Phys. Rev. Lett. **108**, 256808 (2012).

[27] L.X. Yang, G. Rohde, T. Rohwer, A. Stange, K. Hanff, C. Sohrt, L. Rettig, R. Cortés, F. Chen, D.L. Feng, T. Wolf, B. Kamble, I. Eremin, T. Popmintchev, M.M. Murnane, H.C. Kapteyn, L. Kipp, J. Fink, M. Bauer, U. Bovensiepen, and K. Rossnagel, *Ultrafast Modulation of the Chemical Potential in $BaFe_2As_2$ by Coherent Phonons.* Phys. Rev. Lett. **112**, 207001 (2014).

[28] L. Perfetti, P. A. Loukakos, M. Lisowski, U. Bovensiepen, H. Berger, S. Biermann, P. S. Cornaglia, A. Georges, and M. Wolf, *Time evolution of the electronic structure of 1T-TaS_2 through the insulator-metal transition.* Phys. Rev. Lett. **97**, 067402 (2006)

[29] F. Schmitt, P. S. Kirchmann, U. Bovensiepen, R. G. Moore, L. Rettig, M. Krenz, J.-H. Chu, N. Ru, L. Perfetti, D. H. Lu, M. Wolf, I. R. Fisher, Z.-X. Shen, *Transient Electronic Structure and Melting of a Charge Density Wave in $TbTe_3$.* Science **321**, 1649 (2008).

[30] S. Kaiser, C. R. Hunt, D. Nicoletti, W. Hu, I. Gierz, H. Y. Liu, M. Le Tacon, T. Loew, D. Haug, B. Keimer, and A. Cavalleri, *Optically induced coherent transport far above T_c in underdoped $YBa_2Cu_3O_{6+\delta}$.* Phys. Rev. B **89**, 184516 (2014).

[31] R. Mankowsky, A. Subedi, M. Först, S. O. Mariager, M. Chollet, H. T. Lemke, J. S. Robinson, J. M. Glownia, M. P. Minitti, A. Frano, M. Fechner, N. A. Spaldin, T. Loew, B. Keimer, A. Georges, and A. Cavalleri, *Nonlinear lattice dynamics as a basis for enhanced superconductivity in $YBa_2Cu_3O_{6.5}$.* Nature **516**, 71 (2014).

[32] R. T. Scalettar, N. E. Bickers, and D. J. Scalapino, *Competition of pairing and Peierlscharge-density-wave correlations in a two-dimensional electron-phonon model.* Phys. Rev. B **40**, 197 (1989).

[33] F. Marsiglio, *Pairing and charge-density-wave correlations in the Holstein model at half-filling.* Phys. Rev. B **42**, 2416 (1990).

[34] O. Rösch and O. Gunnarsson, *Electron-phonon interaction in the three-band model.* Phys. Rev. B **70**, 224518 (2004).

[35] The dimensionless coupling ξ is defined as $\xi = \frac{g_2}{g_1} = \left(\frac{\hbar}{2M_o\Omega}\right)^{\frac{1}{2}} \frac{\alpha_2}{\alpha_1}$. For a typical transition metal oxide $d_0 \sim 2$ $\mathring{A}$, $\beta = 3.5$, and $\left(\frac{\hbar}{2M_o\Omega}\right)^{\frac{1}{2}} \sim 0.043$ $\mathring{A}$ for an $\Omega = 70$ meV bond-stretching oxygen mode.

[36] C. P. J. Adolphs and M. Berciu, *Single-polaron properties for double-well electron-phonon coupling.* Phys. Rev. B **89**, 035122 (2014).

[37] R. Blankenbecler, D. J. Scalapino, and R. L. Sugar, *Monte Carlo calculations of coupled boson-fermion systems. I.* Phys. Rev. D **24**, 2278 (1981).

[38] S. R. White, D. J. Scalapino, R. L. Sugar, E. Y. Loh, J. E. Gubernatis, and R. T. Scalettar, *Numerical study of the two-dimensional Hubbard model.* Phys. Rev. B **40**, 506 (1989).

[39] C.-C. Chang, S. Gogolenko, J. Perez, Z. Bai, and R. T. Scalettar, *Recent advances in determinant quantum Monte Carlo.* Philosophical Magazine B **95**, 1260 (2013).

[40] E. Y. Loh, Jr., J. E. Gubernatis, R. T. Scalettar, S. R. White, D. J. Scalapino, and R. L. Sugar, *Sign problem in*

the numerical simulation of many-electron systems. Phys. Rev. B **41**, 9301 (1990); V. I. Iglovikov, E. Khatami, R. M. Fye, R. T. Scalettar, *Geometry Dependence of the Sign Problem*. arXiv:1501.02832 (2015).

[41] M. Jarrell and J. E. Gubernatis, *Bayesian Inference and the Analytic Continuation of Imaginary-Time Quantum Monte Carlo Data*. Physics Reports **269**, 133 (1996).

[42] E. A. Nowadnick, S. Johnston, B. Moritz, and T. P. Devereaux, *Renormalization of spectra by phase competition in the half-filled Hubbard-Holstein model*. Phys. Rev. B **91**, 165127 (2015).

[43] L. F. Arsenault, P. Sémon, and A.-M. S. Tremblay, *Benchmark of a modified iterated perturbation theory approach on the fcc lattice at strong coupling*. Phys. Rev. B **86**, 085133 (2012).

[44] A. S. Mishchenko, N. Nagaosa, and N. Prokofev, *Diagrammatic Monte Carlo Method for Many-Polaron Problems*. Phys. Rev. Lett. **113**, 166402 (2014).

[45] N. Trivedi and M. Randeria, *Deviations from Fermi-Liquid Behavior above T_c in 2D Short Coherence Length Superconductors*. Phys. Rev. Lett. **75**, 312 (1995).

[46] This is due to the fact that the average lattice displacement is defined here as an average over all sites in the cluster. In the unordered uniform phase, each site is on average singly occupied. Conversely, in the CDW ordered phase, every second site is doubly occupied in a checkerboard pattern. If the average displacement of a singly occupied site is X_0, and the average displacement of a doubly occupied site is approximately twice this, then the average value of the displacement obtained by averaging over all sites will be $\propto N^2 X_0$ in the high-temperature unordered phase and $\propto \frac{1}{2}N^2(2X_0)$ in the low-temperature CDW phase. As a result, no significant temperate dependence is observed in the cluster averaged $\langle X \rangle$.

[47] M. Hohenadler, H. G. Evertz, and W. von der Linden, *Quantum Monte Carlo and variational approaches to the Holstein model*. Phys. Rev. B **69**, 024301 (2004).

[48] F. Marsiglio in *Electron-phonon interaction in oxide superconductors*. Edited by R. Baquero. World Scientific (1990).

[49] M. Vekić and S. R. White, *Gap formation in the density of states for the Holstein model*. Phys. Rev. B **48**, 7643 (1993).

[50] M. Weber, F. F. Assaad, and M. Hohenadler, *Phonon spectral function of the one-dimensional Holstein-Hubbard model*. arXiv:1504.07446 (2015).